PROCEEDINGS OF SCIENCE

PoS(ICRC2025)396

Simulation study of lateral distribution properties of ultra-high energy cosmic ray air showers for the Telescope Array

---

K. Shinozaki,[a,*] **K. Fujisue,**[b] **M. Przybylak**[c] **and Y. Tsunesada**[d] **on behalf of the Telescope Array Collaboration**

[a] *Astrophysics Division, National Centre for Nuclear Research, Warsaw, Poland*
[b] *Institute of Physics, Academia Sinica, Taipei, Taiwan*
[c] *Doctoral School of Exact and Natural Sciences, University of Lodz, Lodz, Poland*
[d] *Osaka Metropolitan University, Osaka, Japan*

E-mail: `kenji.shinozaki@ncbj.gov.pl`

Ultra-high energy cosmic rays (UHECRs) are extremely rare and of unknown origin. They are studied indirectly via air showers, but the reconstructed energy scale carries intrinsic uncertainties whose causes are not fully understood. We investigate the lateral distribution of particle densities in UHECR-induced showers simulated for the Telescope Array (TA) surface detectors using CORSIKA with QGSJET-II04, EPOS-LHC, and Sibyll 2.3e. Analyzing detector-level simulation outputs without reconstruction eliminates biases from the array layout and algorithms. The results show systematically steeper lateral distributions than the empirical function used in TA analysis. While $S(800)$ remains a robust energy estimator, differences from the currently used look-up table are attributed to idealized versus realistic array assumptions. Hybrid events help calibrate this offset. Dependence on primary particle and interaction model is marginal. These findings support future efforts to derive average lateral distributions from data to constrain related uncertainties.

39th International Cosmic Ray Conference (ICRC2025)
15–24 July 2025
Geneva, Switzerland

ICRC 2025
The Astroparticle Physics Conference
Geneva July 15-24, 2025

---

[*] Speaker

https://pos.sissa.it/

1. Introduction

The nature and origin of ultra-high energy cosmic rays (UHECRs; defined as those with energies above 10^{18} eV) remain open questions in modern astrophysics. Due to their extremely low and rapidly decreasing flux with primary energy E_0, they can only be observed indirectly through the detection of air showers using fluorescence detectors (FDs), or surface detectors (SDs) which are typically deployed with 1–2 km spacing over areas of hundreds to thousands of square kilometers. Currently, the Telescope Array (TA) in Utah, USA, and the Pierre Auger Observatory in Mendoza, Argentina, are operating such UHECR detectors. These experiments have reported UHECR energy spectra, but notable discrepancies exist in the measured flux as TA reports systematically higher values than Auger. This difference can largely be accounted for by a relative energy scale shift of approximately $\pm 4.5\%$ below $\sim 10^{19.5}$ eV [1].

The energy scale is primarily determined using FDs operated during dark nights, which detect fluorescence light emitted by shower particles. The intensity of this light is proportional to the energy deposited in the atmosphere by those particles. The energy of the shower is estimated from the reconstructed longitudinal shower profile, accounting for the fluorescence yield, atmospheric attenuation, and the so-called 'missing energy' carried away by muons and neutrinos and so on.

In contrast, SDs operate continuously day and night to sample secondary particles and measure their density and arrival time. These measurements provide the core position on the ground and the arrival direction of the shower, i.e., the shower axis. As a result, the lateral distribution of particle density ρ as a function of the distance from the axis R can also be obtained. The density at a fixed R, typically several hundred meters to 1 km, correlates with the E_0 and exhibits minimal fluctuation at such distances [2]. Assuming isotropic flux at a given energy, as in the constant intensity cut (CIC) method [3], the observed density attenuates with increasing zenith angle ϑ.

In the TA experiment, we chose the density at 800 m, denoted $S(800)$ [4]. Due to possible deviations from CIC approach, we established the correlation of unknown E_0 with observable $S(800)$ and ϑ of the shower using the Monte Carlo simulation. The results are summarized into 'look-up table' (LUT), which is a function to yield the most probable simulated energy $E_{\mathrm{LUT}}(S(800), \vartheta)$. Such tables vary depending on the SD experiment, analysis method, and simulation assumptions.

To reduce associated biases, E_{LUT} is calibrated by calorimetrically measured energy E_{FD} by FDs in the hybrid events. For the main TA, the scaling factor $E_{\mathrm{LUT}}/E_{\mathrm{FD}}$ was found to be 1.27 [5], which is applied to science analyses like energy spectrum and anisotropy of UHECRs.

In this work, we investigated the observables and related parameters used in the TA SD shower analysis using CORSIKA air shower simulations. By eliminating the experimental constraints such as the array layout and detector resolution, we aim to clarify their intrinsic properties [6]. We also examined the dependence on primary particles between proton and iron and hadronic interaction models, called 'models' hereafter, and discuss implications for the energy scale and SD analysis.

2. Surface detectors of the Telescope Array

In the Telescope Array experiment, three sub-experiments are organized: the main TA, TA×4, and TALE (TA Low-energy Extension; not discussed in this work). The main TA comprises 507 SDs deployed on a square grid with 1.2 km spacing, covering approximately 700 km^2. TA×4 includes up to 500 additional SDs with 2.08 km spacing, deployed in the northeastern and southeastern regions of the main TA; currently, 257 SDs are operational. This extension increased the total SD coverage by about 1000 km^2. Both arrays are located at an altitude of ~1400 m above sea level (asl.).

Each SD [7] consists of two 3 m^2 plastic scintillator layers with a thickness of 1.2 cm, separated by a 1 mm stainless steel plate. Scintillation light is collected via wavelength-shifting fibers connected to photomultiplier tubes whose signals are digitized at a 50 MHz sampling rate. Signals exceeding ~0.3 minimum ionizing particles are recorded as waveforms in both layers when multi-level trigger conditions are met. For showers with $\vartheta < 55^\circ$, the trigger efficiency reaches ~100% at 10^{19} eV for the main TA and 3×10^{19} eV for TA×4.

The integrated waveform is converted into the particle density ρ expressed in units of vertical-equivalent muons (VEMs) per square meter. To determine $S(800)$, the measured lateral distribution is fitted with the lateral distribution function (LDF) as follows [8]:

$$\rho(R) = C \cdot (R/91.6\ [\mathrm{m}])^{-1.2} \cdot (1 + R/91.6\ [\mathrm{m}])^{-(\eta-1.2)} \cdot \left[1 + (R/1\ [\mathrm{km}])^2\right]^{-0.6}, \quad (1)$$

$$\eta(\vartheta) = \eta_0 - \alpha \cdot (\sec\vartheta - 1), \qquad \eta_0 = 3.97 \text{ and } \alpha = 1.79 \text{ for AGASA and TA analyses} \quad (2)$$

where C is the normalization constant. This LDF was obtained by the AGASA experiment operated at ~910 m asl. Its data in the energy regime between ~10^{18} and a few times 10^{19} eV was used and was validated up to $\sec\vartheta \lesssim 1.7$ ($\vartheta \lesssim 54^\circ$).

3. Simulations

Using three different models, QGSJET-II04 [9], EPOS-LHC [10], and Sibyll2.3e [11] with CORSIKA, we generating ~250 events each for proton and iron primaries at fixed energies $E_{\mathrm{MC}} = 10^{18}, 10^{18.5}, \ldots, 10^{20.5}$ eV, assuming isotropic arrival direction up to $\vartheta = 60^\circ$. The thinning option was applied with a level of 10^{-6}, where only one selected particle with a 'weight' assigned is tracked when secondaries below $10^{-6} \cdot E_{\mathrm{MC}}$ are produced.

The particle outputs were processed through 'de-thinning' [12] and SD response simulation [5]. In the former, the weighted particles are spatially re-distributed to cancel the thinning effects. In the latter, the energy deposit of each particle in the scintillator is calculated using tabulated GEANT4 [13] simulation results that account for the SD structure, including the metallic container. As a result, a 'tile file' is produced for each shower, recording the waveforms of all particles reaching the ground level, binned into 6 m grids over a ~14 km×14 km area around the shower core. A large set of such events is formatted in the same way as experimental data, with shower cores placed on the actual SD array layout. Time-dependent calibration is incorporated by sampling from the tile files, and the events are reconstructed using the same procedure as for the real data. Using such end-to-end simulations, the specific LUTs were built for the main TA [5] and TA×4 [14] taking into account their configuration. Hereafter, 'LUT' refers to the one built with proton primary and the QGSJET-II03 model used for the main TA analysis.

In this work, we analyzed only the tile files without further procedures such as reconstruction, focusing mainly on intrinsic properties of the simulated showers about the average lateral distributions and $S(800)$. This approach avoids the existing biases due to the SD array configuration and the uncertainties introduced by the reconstruction process [15–17].

4. Results

Average lateral distributions The average lateral distributions are obtained in $\sec\vartheta$ bins in a step of 0.1 for different combinations of primaries and models. From the corresponding tile files, the average densities, expressed in units of VEM m^{-2}, are calculated in 50 m core distance bins.

Figure 1 shows the results at $E_{\mathrm{MC}} = 10^{18}, 10^{19}$, and 10^{20} eV and the selected $\sec\vartheta$ bins of < 1.1, 1.3–1.4, and 1.5–1.6, for different primaries and models. For comparison, Equation (1) is shown, normalized to $S(800)$ obtained inversely from LUT at the median of each $\sec\vartheta$ bin.

Compared to Equation (1), which represents the LDF used in the SD analysis, the simulations at 10^{19} and 10^{20} eV where the trigger bias is negligible for the main TA show densities near 800 m that closely match those from LUT. The deviations observed between LUT and the simulations primarily reflect different versions of the QGSJET-II model used in this work and in building LUT.

In contrast, at 10^{18} eV, except for the case of $\sec\vartheta = 1.5$–1.6, the simulated lateral distributions show significantly higher densities around the core, including at 800 m. This is likely due to trigger and reconstruction biases at lower energies. At large zenith angles, the trigger efficiency is higher because more SDs are located at small core distances due to the geometry of inclined showers, which helps reduce the discrepancy.

When the overall shape of the lateral distribution is compared with the LDF given by Equations (1) and (2), all simulated results regardless of the primaries or models exhibit a steeper shape, indicating reduced densities at large core distances. Although this is not a direct comparison with experimental data from TA, the observed difference may reflect the so-called muon deficit [18], in which simulations tend to show smaller muon densities. The shape of the lateral distribution can be characterized by fitting the data with the same equations, allowing the η parameter to vary freely.

Figure 2 summarizes η as a function of $\sec\vartheta$ based on the results of Figure 1 and of other $\sec\vartheta$ ranges. Fits on two most extreme cases using Equation (1) are shown for comparison with this equation along with the default coefficients employed in the SD analysis, labeled as 'AGASA'.

Table 1 summarizes the coefficients η_0 and α describing the η parameter based on Figure 2. They are obtained from the fit using Equation (2) in the range of $\sec\vartheta < 2$. In the last row, the average and standard deviation of all simulated combinations are also given to describe discrepancy from default coefficients and dependence among combinations of primaries and models.

The η parameter characterizes the steepness of the LDF and is related to the development stage of the air shower. As the shower propagates through the atmosphere, its particles spread laterally, resulting in a flatter LDF at larger distances from the core, corresponding to smaller values of η. In addition to the zenith angle dependence expressed by Equation (2), η also shows clear dependence between proton and iron, some dependence on energy, particularly for iron or large zenith angles.

As seen in Figure 1, the η values from simulations are already larger than the LDF used in the analysis. At 10^{18} eV around which Equation (2) was experimentally obtained by AGASA, the simulated η_0 values range between 4.3 and 4.7 (not shown in the figure). A part of this difference may result from higher observation level, where the vertical atmospheric depth is ~875 g cm^{-2}, about 95% of that at AGASA. However, it only explains difference in η by ~0.09. In energies above 10^{19} eV, the average η obtained from simulations tends to be larger than those given by Equation (2). Compared to this discrepancy, we found that the dependence on different combinations of primaries and interaction models is marginal.

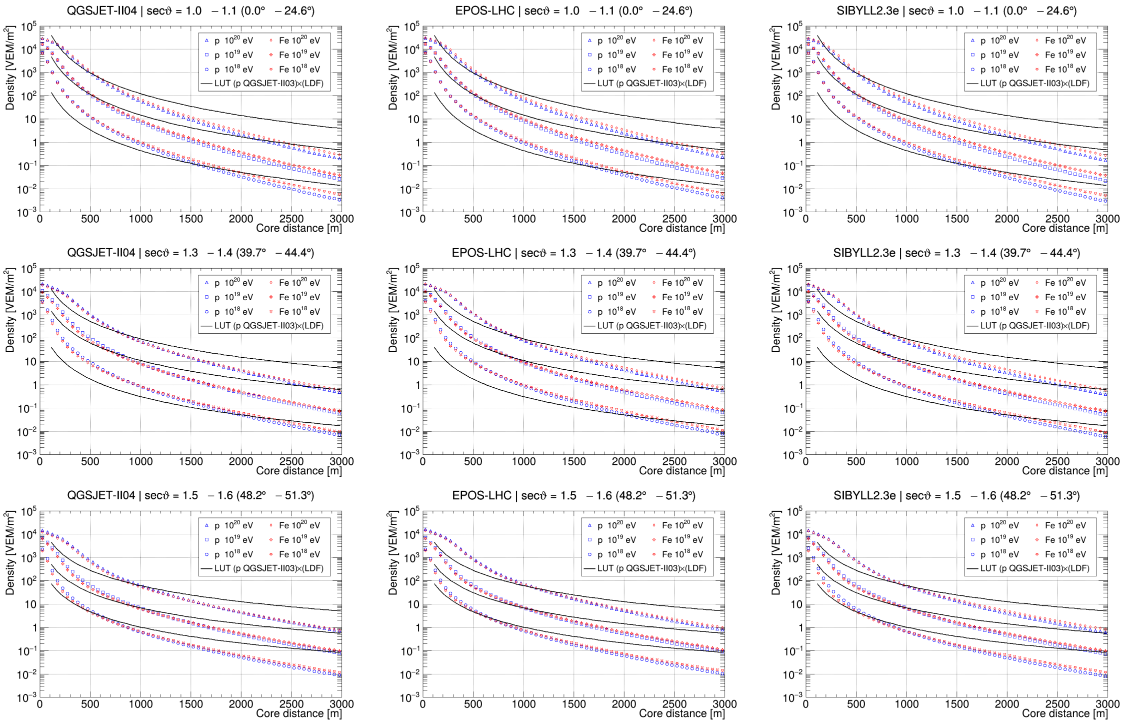

Figure 1: Average lateral distribution of proton and iron showers with $E_{\rm MC}$ = 10^{18}, 10^{19}, and 10^{20} eV as shown in the legend for different $\sec\theta$ ranges, top panels: < 1.1, middle: $1.3 - 1.4$, and bottom: $1.5 - 1.6$ and interaction models, left: QGSJET-II04, middle: EPOS-LHC and right: Sibyll2.3e. The solid curves represent the LDF used in the SD reconstruction by normalizing with the $S(800)$ based on LUT.

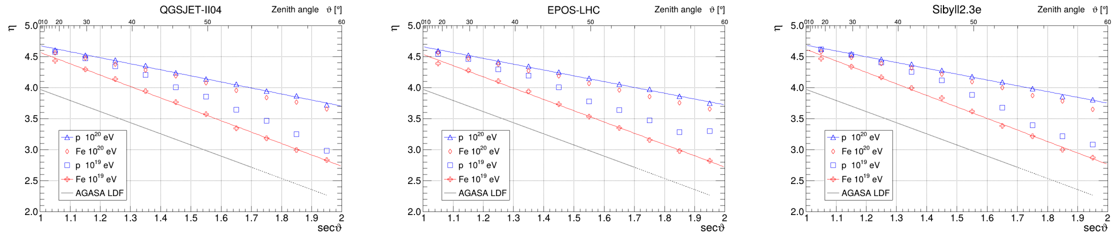

Figure 2: η vs. $\sec\vartheta$ for proton and iron showers at $E_{\rm MC}$ = 10^{19} and 10^{20} eV with different models. For comparison with Equation (2) labeled 'AGASA', fits using this function are shown for the most extreme cases.

Table 1: Summary of the fitted η_0 and α coefficients from the results in Figure 2. The last row describes the discrepancy from default coefficients and dependence among combinations of primaries and models.

Primary	$E_{\rm MC}$ = 10^{19} eV						$E_{\rm MC}$ = 10^{20} eV					
(LDF)	η_0 = 3.97			α = 1.79			η_0 = 3.97			α = 1.79		
(Model)	QGS	EPS	SIB	QGS	EPS	SIB	QGS	EPS	SIB	QGS	EPS	SIB
Proton	4.77	4.67	4.83	1.77	1.53	1.83	4.68	4.66	4.68	0.97	0.94	0.93
Iron	4.57	4.54	4.61	1.83	1.81	1.85	4.63	4.62	4.65	1.03	1.01	1.03
⟨Sim⟩	4.67 ± 0.10			1.77 ± 0.11			4.65 ± 0.02			0.99 ± 0.04		

$S(800)$ vs. $\sec\vartheta$ and E_{MC} relations Using the tile files, $S(800)$ for each shower is calculated by integrating waveform signals in the ring between 700 and 900 m from the shower axis, and then dividing by its area. The $S(800)$ vs. $\sec\vartheta$ relation at fixed energy generally reflects the attenuation of shower particle density as the shower develops deeper in the atmosphere. Without detector bias, a quasi-linear relation between $S(800)$ and E_{MC} at a fixed zenith angle is expressed as: $S(800) = S_{\mathrm{ref}}(800) \cdot (E_{\mathrm{MC}}/E_{\mathrm{ref}})^{\beta}$ with a scaling index $\beta \approx 1$ where $S_{\mathrm{ref}}(800)$ is $S(800)$ at a reference energy E_{ref}.

Figure 3 shows $S(800)$ as a function of zenith angle of the individual simulated showers at 10^{18}, 10^{19}, and 10^{20} eV with different primaries and models. For upper two energies, corresponding $S(800)$ from LUT is compared. The horizontal axis is rescaled to $\sin^2\vartheta$, to account for the solid angle acceptance. The corresponding $\sec\vartheta$ scale is shown on the top.

At energies above 10^{19} eV, simulations show a slight peak near the vertical direction, with iron primaries peaking closer to the zenith than protons, due to differences in shower development profiles. Iron showers also exhibit smaller shower-to-shower fluctuations. The correlation given by LUT intersects the simulated relation at around $\sec\vartheta \sim 1.2$–1.3. At smaller zenith angles, the simulated $S(800)$ is lower than LUT values, while at larger zenith angles, it becomes higher.

Figure 4 shows $S(800)$ vs. E_{MC} relation with different primaries and models in $\sec\vartheta$ ranges of < 1.2, 1.2–1.4, and 1.4–1.6. For each range, a quasi-linear fit is applied on the logarithmic scales.

Table 2 summarizes $S(800)$ values and scaling index β from the fits shown in Figure 4. LUT values are shown for comparison, and the relative differences quantify primary and model dependence based on the mean and standard deviation of the six values in each set.

The $S(800)$ vs. E_{MC} relations are well described by a quasi-linear function with scaling indices slightly larger for iron primary than for proton and in higher zenith angle, reflecting differences in the shower development stage. The relative dependence of $S(800)$ on primaries and models remains within $\pm 13\%$, indicating that $S(800)$ is intrinsically a stable energy estimator.

Discussion A recent study using the QGSJET-II04 model with a proton primary as the LUT for the main TA found a scaling factor of 1.16, based on the $E_{\mathrm{LUT}}/E_{\mathrm{FD}}$ ratio using hybrid events with energies above $\sim 10^{19}$ eV. A similar scaling factor of 1.36 was evaluated for TA×4 by matching the reconstructed energy distribution of simulated showers to that of experimental ones [14]. This approach was adopted due to the limited statistics of hybrid events currently available from TA×4.

Reconstructing the full lateral distribution for each individual shower is not essential, as long as the derived $S(800)$ is sufficiently close to the true value to achieve the scientific objectives. However, applying analysis functions in SD reconstruction that better represent the actual characteristics of air showers may help reduce biases in data interpretation.

In the SD data analysis, LUTs are used and inherently reflect biases from the array layout and reconstruction process. Differences between the LUT and this work, beyond model dependence, are mainly attributed to such biases in determining $S(800)$. Deviations from the assumed LDF, as shown in Figure 1, also contribute. Despite the offset in LUT-based energies, we rescaled E_{LUT} to E_{FD}, which experimentally provides an absolute energy scale. As a cross-check, we applied the CIC method to extract the UHECR energy spectrum without using LUTs, and found agreement in the energy scale within 2% [19]. The distributions of other reconstructed parameters also show good agreement between simulated and observed datasets, further validating the overall procedure.

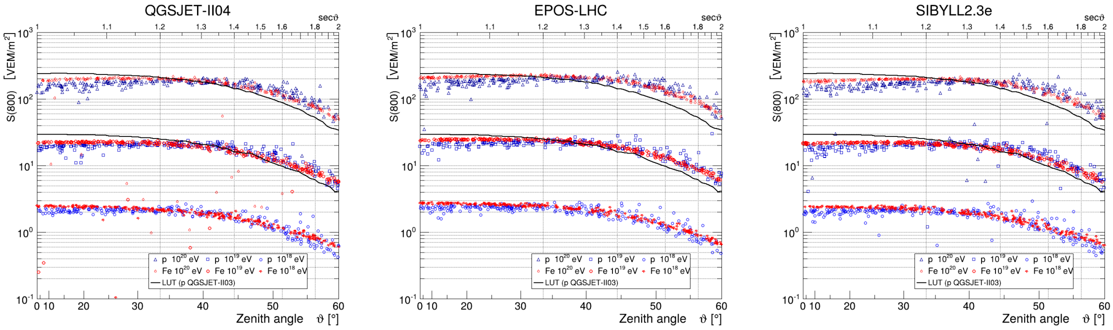
QGSJET-II04 EPOS-LHC SIBYLL2.3e

Figure 3: $S(800)$ as a function of zenith angle for individual simulated showers at 10^{18}, 10^{19}, and 10^{20} eV, for different primary particles and interaction models. For comparison, LUT-based $S(800)$ values are shown for the two higher energies. The horizontal axis is rescaled to $\sin^2\theta$ to reflect solid angle acceptance, and the corresponding $\sec\theta$ values are indicated on the top axis.

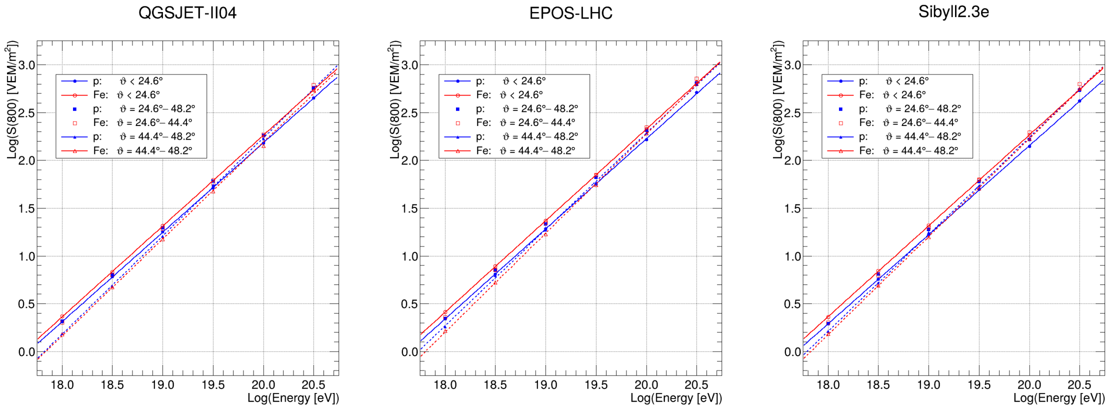
QGSJET-II04 EPOS-LHC Sibyll2.3e

Figure 4: $S(800)$ vs. $E_{\rm MC}$ relation for proton and iron primaries in $\sec\vartheta$ bins of < 1.2, 1.2–1.4, and 1.4–1.6 with different models. For each $\sec\vartheta$ bin, a quasi-linear fit is applied on the logarithmic scales.

Table 2: Summary of the $S(800)$ and β values from the fits in Figure 4. LUT values are compared, and the relative differences quantify primary and model dependence based on the mean of the six values in each set.

$\sec\vartheta$	1ry	$S(800)@E_{\rm MC} = 10^{19}$ eV				$S(800)@E_{\rm MC} = 10^{20}$ eV				β		
		LUT	QGS	EPS	SIB	LUT	QGS	EPS	SIB	QGS	EPS	SIB
1.0 – 1.2	p	28.7	17.7	19.3	16.7	234	154	169	143	0.94	0.94	0.93
	Fe		17.7	23.5	20.7		184	213	185	0.95	0.96	0.95
1.2 – 1.4	p	21.2	19.6	21.5	18.8	185	185	206	174	0.98	0.98	0.97
	Fe		19.4	19.3	19.9		189	223	198	0.98	1.00	1.00
1.4 – 1.6	p	13.7	16.2	22.4	16.9	116	173	193	174	1.03	1.01	1.01
	Fe		15.1	19.3	15.9		156	189	169	1.01	1.04	1.03
		$(\langle\mathrm{Sim}\rangle - \mathrm{LUT})/\langle\mathrm{Sim}\rangle$				$(\langle\mathrm{Sim}\rangle - \mathrm{LUT})/\langle\mathrm{Sim}\rangle$						
1.0 – 1.2		−45% ± 11%				−34% ± 13%						
1.2 – 1.4		−5% ± 6%				+4% ± 11%						
1.4 – 1.6		+15% ± 10%				+36% ± 7%						

5. Summary

We investigated the intrinsic properties of the lateral distribution of particle densities in proton and iron induced air showers simulated for the main TA and TA×4 SD arrays using CORSIKA with QGSJET-II-04, EPOS-LHC, and Sibyll 2.3e. Compared with the formula used in the analysis, all simulations exhibit a steeper lateral distribution. The dependence of $S(800)$ on the zenith angle was also examined as an energy estimator.

Systematic discrepancies with the current LUT used in the SD analysis were identified. However, they are largely compensated by hybrid events, which calibrate the energy scale and validate the overall analysis procedure. The dependence on the primary particle type and hadronic interaction model was found to be marginal compared to other uncertainties.

In future studies, we aim to extract average LDFs from experimental data to better understand and constrain related uncertainties to include into the data analysis.

References

[1] R.U. Abbasi et al. (2024), arXiv:2406.08612.

[2] A.M. Hillas et al. (1971), Proc. 12th Int. Cosmic Ray Conf. (Hobart), 3, 1001.

[3] T.K. Gaisser and A.M. Hillas (1977), in Proc. 15th Int. Cosmic Ray Conf. (Plovdiv), 8, 353.

[4] A. Taketa (2012), PhD Thesis; University of Tokyo.

[5] K. Ivanov (2012), PhD Thesis; Rutgers, the State University of New Jersey.

[6] D. Heck et al. (1998), Forschungszentrum Karlsruhe Report FZKA 6019.

[7] T. Abu-Zayyad et al. (2012), Nucl. Instrum. Meth. A689, 87.

[8] S. Yoshida et al. (1994), J. Phys. G: Nucl. Part. Phys. 20, 651.

[9] S. Opstachenko (2011), Phys. Rev. D83, 014018.

[10] T. Pierog et al. (2015), Phys. Rev. C92, 034906.

[11] F. Riehn et al. (2020), Phys. Rev. D102, 063002.

[12] B.T. Stokes et al. (2012), Astropart. Phys. 35, 759.

[13] J. Allison J. et al. (2016), Nucl. Instrum. Meth. A835, 186.

[14] K. Fujisue (2024), PhD Thesis; University of Tokyo.

[15] C. Koyama et al. (2025), in these proceedings.

[16] R. Sakamoto et al. (2025), in these proceedings.

[17] K. Fujisue et al. (2025), in these proceedings.

[18] D. Góra (2024), SciPost Phys. Proc. 15, 020.

[19] J.H. Kim et al.(2023), EPJ Web Conf. 283, 02005.

Full Authors List: The Telescope Array Collaboration

R.U. Abbasi[1], T. Abu-Zayyad[1,2], M. Allen[2], J.W. Belz[2], D.R. Bergman[2], F. Bradfield[3], I. Buckland[2], W. Campbell[2], B.G. Cheon[4], K. Endo[3], A. Fedynitch[5,6], T. Fujii[3,7], K. Fujisue[5,6], K. Fujita[5], M. Fukushima[5], G. Furlich[2], Z. Gerber[2], N. Globus[8], T. Hanaoka[9], W. Hanlon[2], N. Hayashida[10], H. He[11*], K. Hibino[10], R. Higuchi[11], D. Ikeda[10], D. Ivanov[2], S. Jeong[12], C.C.H. Jui[2], K. Kadota[13], F. Kakimoto[10], O. Kalashev[14], K. Kasahara[15], Y. Kawachi[3], K. Kawata[5], I. Kharuk[14], E. Kido[5], H.B. Kim[4], J.H. Kim[2], J.H. Kim[2†], S.W. Kim[12‡], R. Kobo[3], I. Komae[3], K. Komatsu[16], K. Komori[9], A. Korochkin[17], C. Koyama[5], M. Kudenko[14], M. Kuroiwa[16], Y. Kusumori[9], M. Kuznetsov[14], Y.J. Kwon[18], K.H. Lee[4], M.J. Lee[12], B. Lubsandorzhiev[14], J.P. Lundquist[2,19], H. Matsushita[3], A. Matsuzawa[16], J.A. Matthews[2], J.N. Matthews[2], K. Mizuno[16], M. Mori[9], S. Nagataki[11], K. Nakagawa[3], M. Nakahara[3], H. Nakamura[9], T. Nakamura[20], T. Nakayama[16], Y. Nakayama[9], K. Nakazawa[9], T. Nonaka[5], S. Ogio[5], H. Ohoka[5], N. Okazaki[5], M. Onishi[5], A. Oshima[21], H. Oshima[5], S. Ozawa[22], I.H. Park[12], K.Y. Park[4], M. Potts[2], M. Przybylak[23], M.S. Pshirkov[14,24], J. Remington[2§], C. Rott[2], G.I. Rubtsov[14], D. Ryu[25], H. Sagawa[5], N. Sakaki[5], R. Sakamoto[9], T. Sako[5], N. Sakurai[5], S. Sakurai[3], D. Sato[16], K. Sekino[5], T. Shibata[5], J. Shikita[3], H. Shimodaira[5], H.S. Shin[3,7], K. Shinozaki[26], J.D. Smith[2], P. Sokolsky[2], B.T. Stokes[2], T.A. Stroman[2], H. Tachibana[3], K. Takahashi[5], M. Takeda[5], R. Takeishi[5], A. Taketa[27], M. Takita[5], Y. Tameda[9], K. Tanaka[28], M. Tanaka[29], M. Teramoto[9], S.B. Thomas[2], G.B. Thomson[2], P. Tinyakov[14,17], I. Tkachev[14], T. Tomida[16], S. Troitsky[14], Y. Tsunesada[3,7], S. Udo[10], F. Urban[30], A. Urena[30], M. Vrábel[26], D. Warren[11], K. Yamazaki[21], Y. Zhezher[5,14], Z. Zundel[2], and J. Zvirzdin[2]

[1] Department of Physics, Loyola University-Chicago, Chicago, Illinois 60660, USA
[2] High Energy Astrophysics Institute and Department of Physics and Astronomy, University of Utah, Salt Lake City, Utah 84112-0830, USA
[3] Graduate School of Science, Osaka Metropolitan University, Sugimoto, Sumiyoshi, Osaka 558-8585, Japan
[4] Department of Physics and The Research Institute of Natural Science, Hanyang University, Seongdong-gu, Seoul 426-791, Korea
[5] Institute for Cosmic Ray Research, University of Tokyo, Kashiwa, Chiba 277-8582, Japan
[6] Institute of Physics, Academia Sinica, Taipei City 115201, Taiwan
[7] Nambu Yoichiro Institute of Theoretical and Experimental Physics, Osaka Metropolitan University, Sugimoto, Sumiyoshi, Osaka 558-8585, Japan
[8] Institute of Astronomy, National Autonomous University of Mexico Ensenada Campus, Ensenada, BC 22860, Mexico
[9] Graduate School of Engineering, Osaka Electro-Communication University, Neyagawa-shi, Osaka 572-8530, Japan
[10] Faculty of Engineering, Kanagawa University, Yokohama, Kanagawa 221-8686, Japan
[11] Astrophysical Big Bang Laboratory, RIKEN, Wako, Saitama 351-0198, Japan
[12] Department of Physics, Sungkyunkwan University, Jang-an-gu, Suwon 16419, Korea
[13] Department of Physics, Tokyo City University, Setagaya-ku, Tokyo 158-8557, Japan
[14] Institute for Nuclear Research of the Russian Academy of Sciences, Moscow 117312, Russia
[15] Faculty of Systems Engineering and Science, Shibaura Institute of Technology, Minumaku, Tokyo 337-8570, Japan
[16] Academic Assembly School of Science and Technology Institute of Engineering, Shinshu University, Nagano, Nagano 380-8554, Japan
[17] Service de Physique Théorique, Université Libre de Bruxelles, Brussels 1050, Belgium
[18] Department of Physics, Yonsei University, Seodaemun-gu, Seoul 120-749, Korea
[19] Center for Astrophysics and Cosmology, University of Nova Gorica, Nova Gorica 5297, Slovenia
[20] Faculty of Science, Kochi University, Kochi, Kochi 780-8520, Japan
[21] College of Science and Engineering, Chubu University, Kasugai, Aichi 487-8501, Japan
[22] Quantum ICT Advanced Development Center, National Institute for Information and Communications Technology, Koganei,

---

[*] Presently at: Purple Mountain Observatory, Nanjing 210023, China

[†] Presently at: Physics Department, Brookhaven National Laboratory, Upton, NY 11973, USA

[‡] Presently at: Korea Institute of Geoscience and Mineral Resources, Daejeon, 34132, Korea

[§] Presently at: NASA Marshall Space Flight Center, Huntsville, Alabama 35812, USA

Tokyo 184-8795, Japan
[23] Doctoral School of Exact and Natural Sciences, University of Łódź, Łódź, Łódź 90-237, Poland
[24] Sternberg Astronomical Institute, Moscow M.V. Lomonosov State University, Moscow 119991, Russia
[25] Department of Physics, School of Natural Sciences, Ulsan National Institute of Science and Technology, UNIST-gil, Ulsan 689-798, Korea
[26] Astrophysics Division, National Centre for Nuclear Research, Warsaw 02-093, Poland
[27] Earthquake Research Institute, University of Tokyo, Bunkyo-ku, Tokyo 277-8582, Japan
[28] Graduate School of Information Sciences, Hiroshima City University, Hiroshima, Hiroshima 731-3194, Japan
[29] Institute of Particle and Nuclear Studies, KEK, Tsukuba, Ibaraki 305-0801, Japan
[30] CEICO, Institute of Physics, Czech Academy of Sciences, Prague 182 21, Czech Republic

Acknowledgements

The Telescope Array experiment is supported by the Japan Society for the Promotion of Science (JSPS) through Grants-in-Aid for Priority Area 431, for Specially Promoted Research JP21000002, for Scientific Research (S) JP19104006, for Specially Promoted Research JP15H05693, for Scientific Research (S) JP19H05607, for Scientific Research (S) JP15H05741, for Science Research (A) JP18H03705, for Young Scientists (A) JPH26707011, and for Fostering Joint International Research (B) JP19KK0074, by the joint research program of the Institute for Cosmic Ray Research (ICRR), The University of Tokyo; by the Pioneering Program of RIKEN for the Evolution of Matter in the Universe (r-EMU); by the U.S. National Science Foundation awards PHY-1806797, PHY-2012934, PHY-2112904, PHY-2209583, PHY-2209584, and PHY-2310163, as well as AGS-1613260, AGS-1844306, and AGS-2112709; by the National Research Foundation of Korea (2017K1A4A3015188, 2020R1A2C1008230, and RS-2025-00556637) ; by the Ministry of Science and Higher Education of the Russian Federation under the contract 075-15-2024-541, IISN project No. 4.4501.18, by the Belgian Science Policy under IUAP VII/37 (ULB), by National Science Centre in Poland grant 2020/37/B/ST9/01821, by the European Union and Czech Ministry of Education, Youth and Sports through the FORTE project No. CZ.02.01.01/00/22_008/0004632, and by the Simons Foundation (00001470, NG). This work was partially supported by the grants of the joint research program of the Institute for Space-Earth Environmental Research, Nagoya University and Inter-University Research Program of the Institute for Cosmic Ray Research of University of Tokyo. The foundations of Dr Ezekiel R. and Edna Wattis Dumke, Willard L. Eccles, and George S. and Dolores Doré Eccles all helped with generous donations. The State of Utah supported the project through its Economic Development Board, and the University of Utah through the Office of the Vice President for Research. The experimental site became available through the cooperation of the Utah School and Institutional Trust Lands Administration (SITLA), U.S. Bureau of Land Management (BLM), and the U.S. Air Force. We appreciate the assistance of the State of Utah and Fillmore offices of the BLM in crafting the Plan of Development for the site. We thank Patrick A. Shea who assisted the collaboration with much valuable advice and provided support for the collaboration's efforts. The people and the officials of Millard County, Utah have been a source of steadfast and warm support for our work which we greatly appreciate. We are indebted to the Millard County Road Department for their efforts to maintain and clear the roads which get us to our sites. We gratefully acknowledge the contribution from the technical staffs of our home institutions. An allocation of computing resources from the Center for High Performance Computing at the University of Utah as well as the Academia Sinica Grid Computing Center (ASGC) is gratefully acknowledged.